ELECTRONIC SUPPLEMENTARY INFORMATION (ESI)

Probing magnetic coupling between $LnPc_2$ (Ln=Tb, Er) molecules and graphene / Ni(111) substrate with and without Au-intercalation: role of the dipolar field.

V. Corradini[1], A. Candini[1*], D. Klar[2], R. Biagi[1,3], V. De Renzi[1,3], A. Lodi Rizzini[1,3,8], N. Cavani[1,3], U. del Pennino[1,3], S. Klyatskaya[4], M. Ruben[4,5], E. Velez-Fort[6], K. Kummer[6], N. B. Brookes[6], P. Gargiani,[7] H. Wende[2], M. Affronte[1,3]

[1]Centro S3, Istituto Nanoscienze - CNR, via G. Campi 213/A , 41125 Modena. Italy.

[2]Faculty of Physics and Center for Nanointegration Duisburg-Essen (CENIDE), University of Duisburg-Essen, Lotharstraße 1, D-47048 Duisburg, Germany

[3]Dipartimento di Scienze Fisiche, Matematiche e Informatiche, Università di Modena e Reggio Emilia via G. Campi 213/A , 41125/A Modena. Italy.

[4]Institute of Nanotechnology, Karlsruhe Institute of Technology (KIT), D-76344 Eggenstein-Leopoldshafen, Germany

[5]Institut de Physique et Chimie des Mat´eriaux de Strasbourg, UMR 7504 UdS-CNRS, 67034 Strasbourg Cedex 2, France

[6]European Synchrotron Radiation Facility (ESRF), Avenue des Martyrs 71, 38043 Grenoble, France

[7] ALBA Synchrotron Light Source, E-08290 Barcelona, Spain

[8] CNR-IOM, Laboratorio TASC, Area Science Park, S.S. 14, km 163.5, 34012 Basovizza (Trieste), Italy

* present affiliation: Istituto di Sintesi Organica e Fotoreattività (ISOF), Consiglio Nazionale delle Ricerche (CNR), Via Gobetti 101, 40129 Bologna, Italy

1. Experimental details: LEED-XPS

Single crystal Ni(111) was cleaned by repeated cycles of sputtering and annealing at 840°C in UHV until a sharp hexagonal LEED pattern was observed (see Fig.S1a). For the graphene layer growth, we follow the procedure reported in literature [S01,S02,S03]. Initially, a freshly prepared Ni(111) surface was heated and stabilized at the synthesis temperature of 500°C. Then, propylene gas (C_3H_6), used as the carbon source, was introduced into the chamber and the pressure adjusted to 2×10^{-7} mbar.

The evolution of the carbon layer has been monitored through X-ray Photoemission Spectroscopy (XPS) following the C-1s spectra evolution as a function of time (fig.S1d). A distinct peak (C_{carb} at 283.2eV) appears after a deposition time of 5 min, which is assigned to nickel carbide or, most probably to C_3H_6 fragments [S03]. For longer deposition time, the characteristic peak of graphene (C_{graph} at 284.7eV) starts to grow. The completion of a single layer of graphene (SLG) after 15min of propylene supply is evidenced by the saturation of the C_{graph} peak and by the LEED image, fig.S1b, which shows a sharp hexagonal pattern characteristic of the 1×1 reconstruction. The presence of the single peak C_{graph} in the C-1s core levels (fig.S1d) proves the high quality, homogeneity, and cleanliness of the SLG.

The Au intercalation below the SLG on Ni(111) was carried out by evaporating 1 ML thick layer of gold (estimated by a quartz microbalance) and subsequent annealing for 10min at 430°C as described in Ref [S04,S05]. The quality, homogeneity, and cleanliness of the prepared SLG/Au/Ni(111) system were checked by LEED (see fig.S1c) and by XPS of the C-1s and Au-4f core levels (see fig.S1d and S1e respectively). After the Au intercalation the C-1s shifts from 284.7 eV (strongly interacting graphene) to 284.3 eV (C_{Au}), that correspond to the non interacting free standing graphene. The good LEED pattern (fig.S1c) and the presence of the single peak C_{Au} in the C-1s core levels unambiguously demonstrate the high quality of the SLG/Au interface.

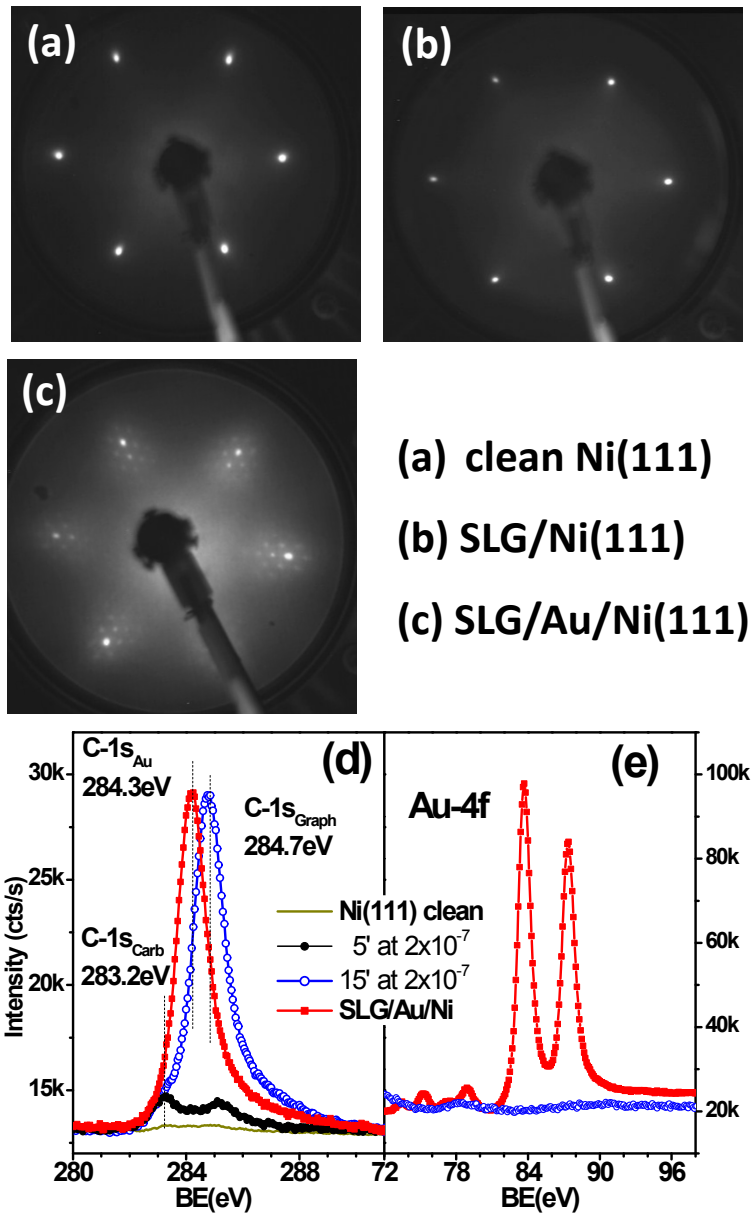

Fig.S1: LEED patterns (primary energy of 150 eV) measured at different steps of the preparation of Au-intercalated graphene on Ni(111) crystal. (a) Clean Ni(111) surface, (b) uniform monolayer graphene (SLG) covering Ni(111) surface. (c) gold intercalated SLG on Ni(111). XPS spectra used to monitor the process evolution: (d) C-1s core level as a function exposure time to propylene gas (P_{prop}= 2x10^{-7}mbar) with the substrate kept at 500°C. The completion of the SLG is evidenced by the saturation of the C_{graph} peak after 15 minutes of exposure. After the Au intercalation the C-1s shifts from 284.7 eV (strongly interacting graphene) to 284.3 eV (C_{Au} peak), that correspond to the non interacting free standing graphene. (e) Au-4f spectra relative to the 1 ML of gold intercalated under the SLG layer (after the annealing for 10 min at 430 °C).

2. ARPES investigation

Fig.S2 shows our Angle-Resolved Photoemission Spectra (ARPES) around the K point of the Brillouin zone of the SLG/Au/Ni(111) system measured at 62eV Photon Energy. The effect of the Au-intercalation on the SLG is found in excellent agreement with what reported in literature [S05, S04]. More specifically, the ARPE-spectrum shows that the electronic band dispersion of graphene on Ni(111), along the direction perpendicular to Γ-K, resembles the one of the freestanding graphene after the intercalation with 1 ML of Au [S06,S07, S04]. The π-states recover the typical linear dependence around the *K* point, with the Dirac cone vertex located very near the Fermi level. Au-5d states appear at much lower energy and this situation suggests a good degree of decoupling of the graphene from the underlying magnetic Ni substrate.

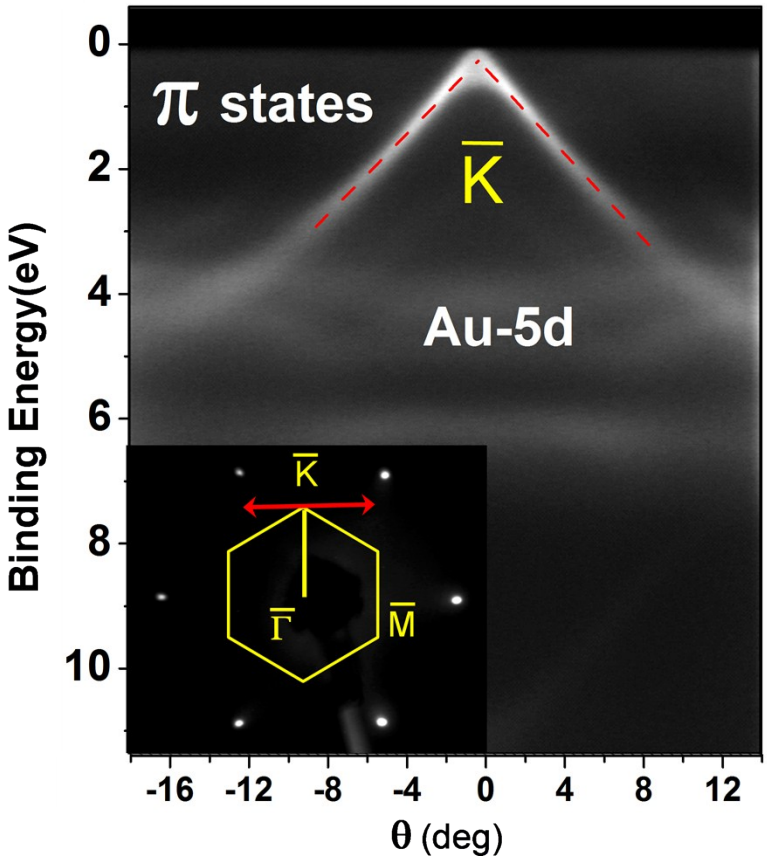

***Fig.S2**_ARPES Angle-resolved photoemission spectrum around the K point of the Brillouin zone of the SLG/Au/Ni(111) system taken at 62eV Photon Energy. The π-band dispersion (dashed red line) along the direction perpendicular to Γ-K (red solid line with the two arrows) after intercalation with 1 ML of Au, resembles the one of the freestanding graphene [ref.S04]*

3. STM investigation

After the deposition of the $LnPc_2$ molecules on the SLG/Ni substrate, STM images (see Fig.S3) show isolated spots with reproducible lateral size of 2-3 nm and height of 0.3-0.4 nm, compatible with the molecule sizes (s3e), assuming that the Pc ring lay flat on the surface. From a statistical analysis applied to the STM images we derived that about 20–40% of the surface is occupied by a 2D distribution of isolated clusters.

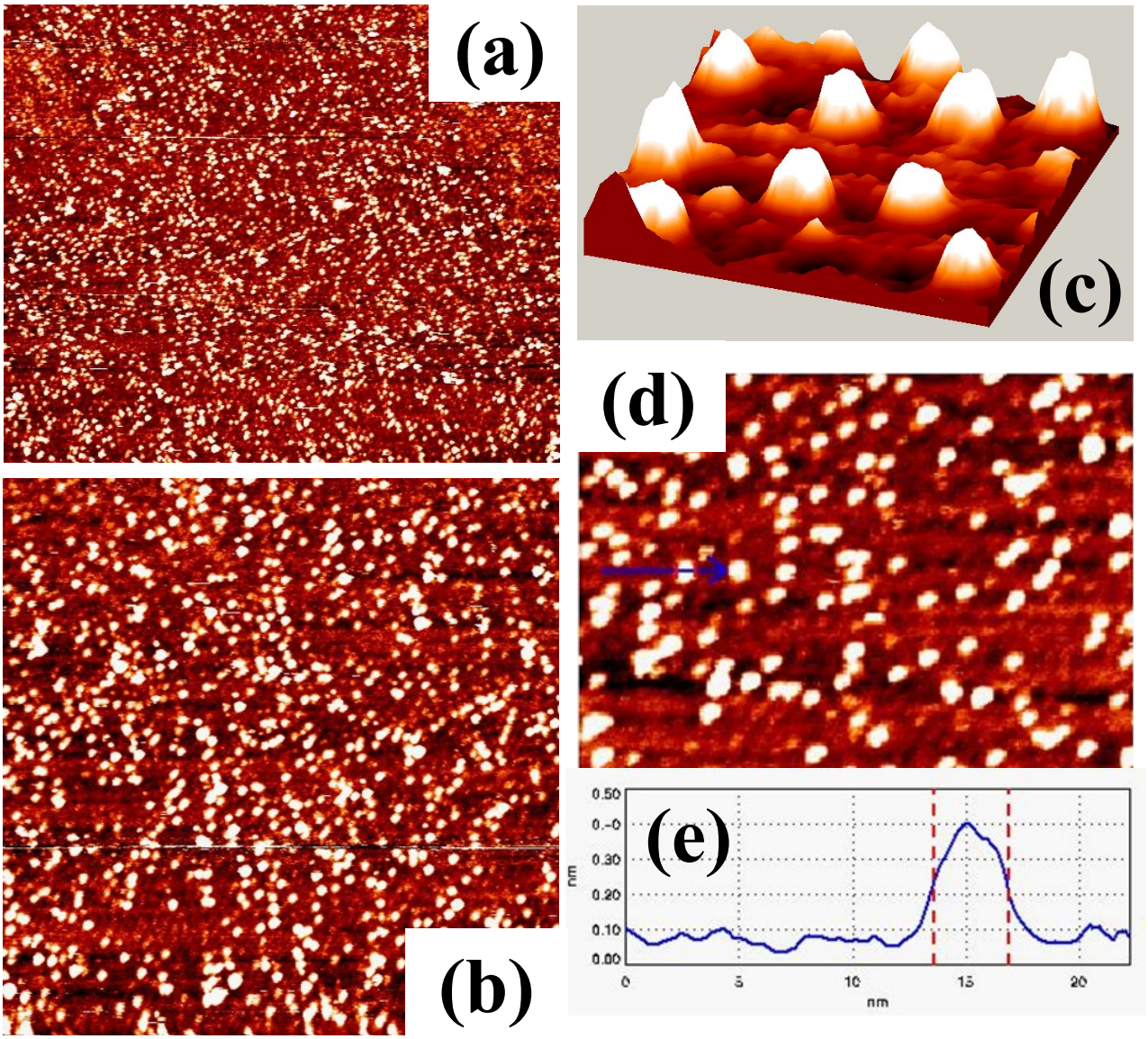

Fig.S3 STM images of isolated Pc_2Tb deposited on the SLG/Ni(111) surface (tunneling conditions: 2 V and 20 pA): (a) (300x250nm2), (b) (200x200nm2), (d) (100x70nm2), (e) height profile measured along the line in panel (d), (c) 3D view of the isolated Pc_2Tb on SLG/Ni(111) surface (25x25nm2)

4. XAS-XMCD investigation

Fig.S4 shows that the shape of the normalized dichroic signal at the Er-M_5 edge does not change with temperature and magnetic field intensity.

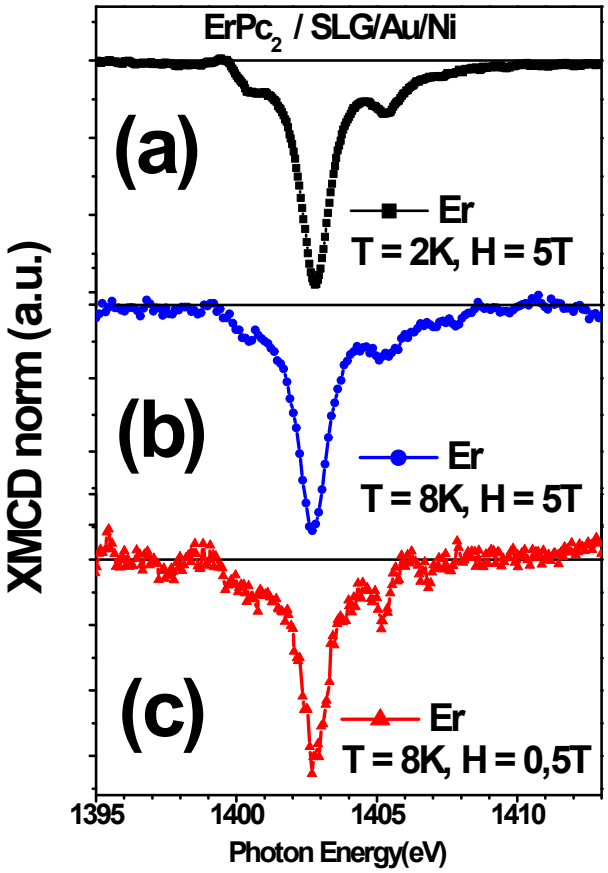

Fig.S4. Comparison between the normalized XMCD spectra at the Er-M_5 edge for the $ErPc_2$ on SLG/Au/Ni(111) measured at H= 5T , T= 2K (panel a), at H= 5T , T= 8K (panel b) and at H= 0.5T , T= 8K (panel c). Measurement conditions: ϑ =70°.

Fig.S5 shows the magnetization curves M(**B**) measured at the M_5 edge at normal incidence (θ = 0°) for $TbPc_2$ deposited on bare Ni (panel (a)), on SLG/Ni(111) ((panel (b)), on SLG/Au/Ni(111) (panel (c)) and at the Ni edge (panel (d)).

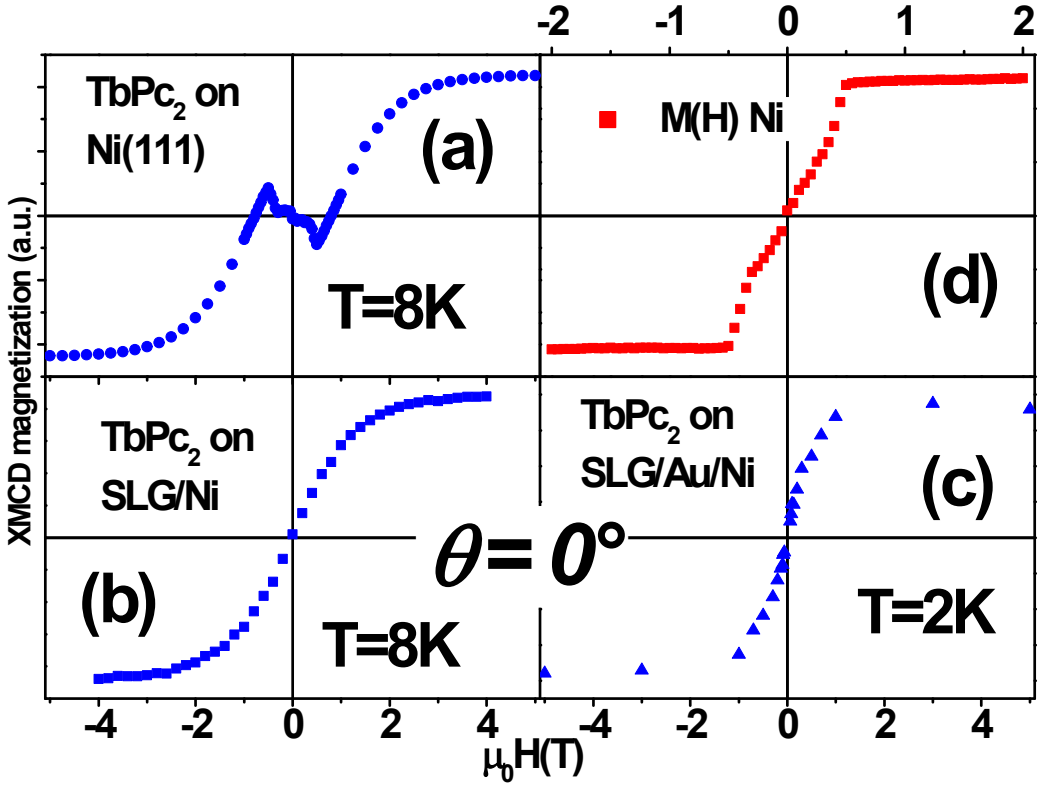

Fig.S5 *Comparison between the magnetization curves at the Tb-M_5 edge measured for the $LnPc_2$ molecules deposited directly on Ni (filled circle symbols in panel a), on SLG/Ni (111) (square symbols in panel b) and on SLG/Au/Ni(111) (triangle symbols in panel c) , measured at normal incident angle (ϑ = 0°). As a reference, in panel (d) is shown the hysteresis of the two Ni(111) single crystal at (ϑ = 0°). Data from panels a,b are taken from references [S08 and S09], respectively. The temperature is 8K for all the measurements performed at ID08-ID32 beamlines (panels a, b, d) while, in panel c, measured at Boreas beamline, T is 2K.*

Fig.S6 shows the magnetization curves M(**B**) measured at the M_5 edge at grazing angle for $TbPc_2$ (upper panels) and $ErPc_2$ (lower panels) deposited on bare Ni, on SLG/Ni(111) and on SLG/Au/Ni(111), from left to right. The sample temperature was 8K in all the measurements performed at ID08-ID32 beamlines (panels a, b, d and e) and 2K at Boreas beamline (panel c). Panel (f) shows the comparison between the magnetization curves taken on $ErPc_2$/SLG/Au/Ni(111) at ID32 (8K) and Boreas (2K). The magnetization behaviour is very similar in both cases and the differences can be ascribed to the different temperature only. In particular, we found that in the low field region (see inset) the two curves are nearly indistinguishable.

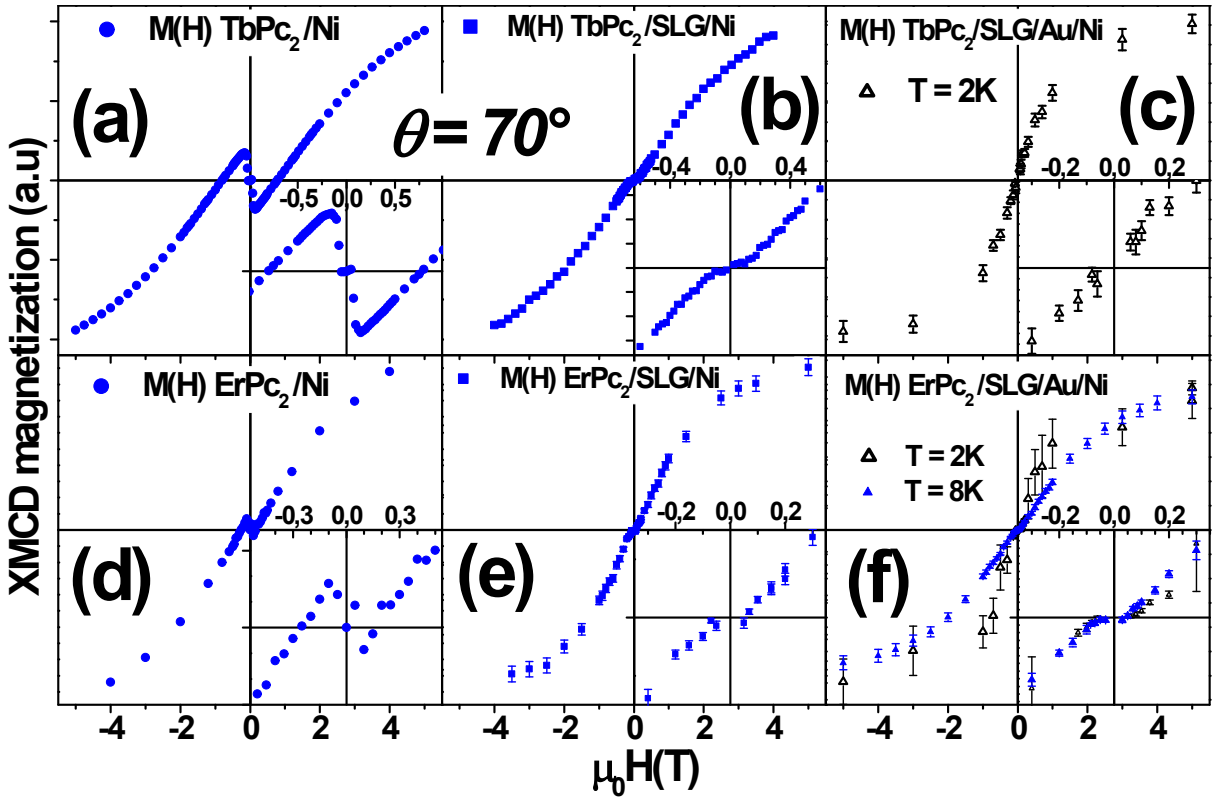

Fig.S6 *Comparison between the magnetization curves at the Ln-$M_{4,5}$ edges (Tb (upper panels) and Er (lower panels) measured for the $LnPc_2$ molecules deposited directly on Ni (filled circle symbols in panels a and d), on SLG/Ni (111) (square symbols in panels b and e) and on SLG/Au/Ni(111) (triangle symbols in panels c and f) , measured at grazing incident angle (ϑ = 70°). Data from panels a,b and d are taken from references [S08 and S09], respectively. Insets: magnification of the low field region. The temperature is 8K for all the measurements performed at ID08-ID32 beamlines (panels a, b, d and e) while, in panel c, measured at Boreas beamline, T is 2K. In f the magnetization curves taken at ID32 (8K) and Boreas (2K) are compared. Here the two curves are normalized to the high field values.*

XMCD analysis at low field.

We here to briefly illustrate the method we devise to extract reliable XMCD intensity values even at very low fields, where the dichroic signal is extremely small and we have to face the problem of signal-to-noise ratio (SNR). The procedure is illustrated in Fig.s7, where the XMCD spectra measured at the Er-M_5 edge are reported for fields spanning from -0.2 T to 0.2 T. Below 0.1 T the dichroic signal is really tiny, and, despite the long measuring time (we averaged tens of spectra), the SNR is still unsatisfactory. In order to extract reliable information from these spectra, we fit each of them with the same fixed spectral lineshape (previously determined by fitting the spectrum taken at 5T), the only fitting parameter being its height. In this way, a statistically objective and, then, reliable estimate of the XMCD intensity (corresponding to the height of the fitting lineshape) and of its uncertainty were obtained. The same procedure was also followed in the case of $TbPc_2$.

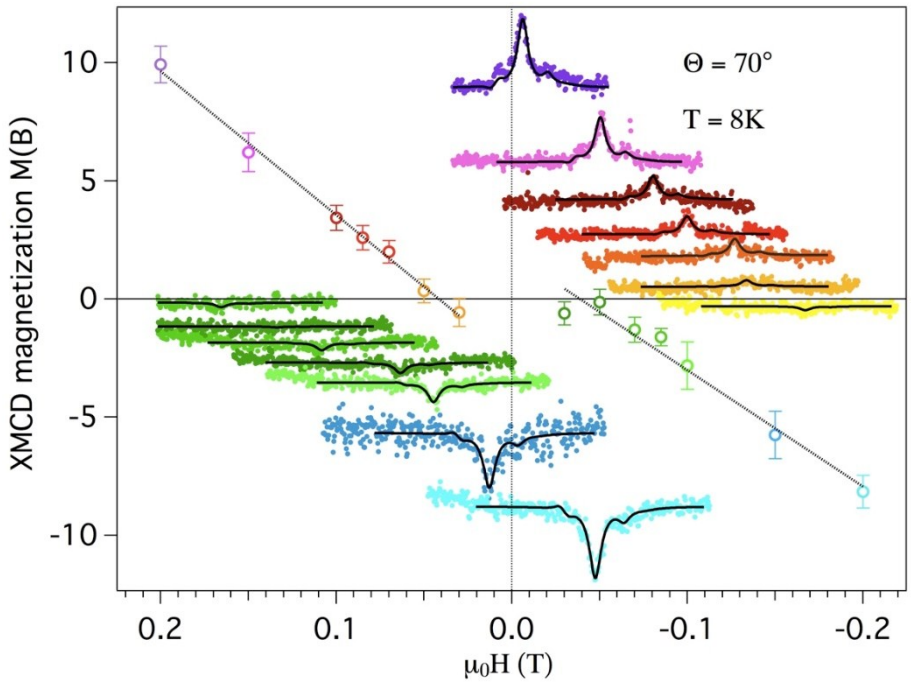

Fig.s7 *$ErPc_2$ molecules deposited on SLG/Au/Ni(111). Er-M_5 magnetization curve (circle symbols) (y-axis, label on the left) and the XMCD spectra corresponding to each point (y-axis, label on the right) in the low field region. For each point of the magnetization curve is reported the experimental XMCD spectrum together with its best-fit (see text for details) which provides the XMCD value. Measurement conditions: temperature 8K, grazing incidence (ϑ = 70°).*

5. Evaluation of the Stray-field of a disc-shaped Ni single crystal

The order of magnitude of the stray field felt by the Ln-molecules deposited at a distance d from the surface of a Nickel single crystal can be estimated in the simplest approximation calculating the field

produced by a uniform collection of magnetic dipoles, each of which is associated to a single atom of the Ni sample. The field associated to a single atomic dipole μ is given by:

$$\vec{B}(\vec{r}) = \frac{\mu_0 \mu_B}{4\pi}\left[\frac{3(\vec{\mu}\cdot\vec{r})\vec{r}}{r^{5/2}} - \frac{\vec{\mu}}{r^{3/2}}\right].$$

The total field of a uniformly magnetized Ni crystal is thus obtained by summing over all atoms in the sample volume, assuming that each Ni dipole moment amounts to a Bohr magneton μ_B.

The field B at an arbitrary position r_0 is therefore given by:

$$\vec{B}(\vec{r_0}) = \frac{\mu_0 \mu_B}{4\pi V_{cell}} \int_V \left[\frac{3(\vec{\mu}\cdot(\vec{r}-\vec{r_0}))(\vec{r}-\vec{r_0})}{(r-r_0)^{5/2}} - \frac{\vec{\mu}}{(r-r_0)^{3/2}}\right] dr,$$

where Vcell = $a_0^3/4$ is the volume of the unitary cell of the Ni crystal, a_0 = 3.524 10^{-10} m being the lattice constant of the Ni fcc crystal. It is worth noting here that in the case of a Nickel sample, the factor $\mu_B\mu_o / 4\pi V_{cell}$ amounts to 84 mT, a value which is of the same order of magnitude of the measured B_{eff} : even without performing the whole calculation, this already suggests that the dipole field cannot be safely disregarded, when trying to explain the experimental results reported in the paper.

In the case of a disc-shaped sample, the value of $B(r_0)$ can be easily computed, introducing cylindrical coordinates (ρ,z), for all positions r_0 = (0, d) along the crystal axis, as shown in

Fig.S8.

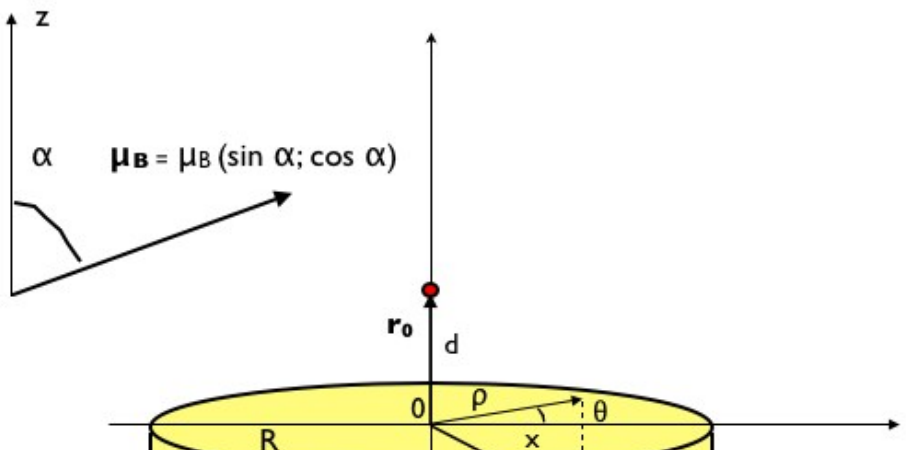

Fig.S8 *Scheme showing the cylindrical coordinates used in the integral calculations. The red circle individuates* ***r0 = (0; d)****, i.e. the point, along the sample axis, at which the field is calculated. R and D are respectively the radius and the thickness of the disc-shaped sample. For sake of clarity, the dimensions (R, D, and d) are not drawn in scale. The orientation of atomic magnetic dipoles* μ_B *relative to the normal direction z are also shown.*

Assuming that the Ni dipole moments are all oriented along the external field (i.e. . $(\mu_x, \mu_y) = \mu_B$ (sinα,cosα), where α= 70° relative to the surface normal), we calculate the surface and normal component of the dipole field as:

$$B_x((0,d)) = \frac{\mu_0\mu_B}{4\pi V_{cell}} \int_0^{2\pi}\int_0^{R}\int_{-D}^{0} [\frac{3\rho^2\cos^2(\theta)\sin\alpha}{(\rho^2+(z-d)^2)^{5/2}} - \frac{\sin\alpha}{(\rho^2+(z-d)^2)^{3/2}}]\rho d\rho d\theta dz =$$

$$= -\frac{\mu_0\mu_B}{4\pi V_{cell}}\sin\alpha\left[\frac{\pi(z-d)}{\sqrt{R^2+(z-d)^2}}\right]_{-D}^{0}$$

and

$$B_z((0,d)) = \frac{\mu_0\mu_B}{4\pi V_{cell}} \int_V [\frac{3z^2\cos\alpha}{(\rho^2+(z-d)^2)^{5/2}} - \frac{\cos\alpha}{(\rho^2+(z-d)^2)^{3/2}}]\rho d\rho d\theta dz =$$

$$= \frac{\mu_0\mu_B}{4\pi V_{cell}} cos\alpha\left[\frac{2\pi(z-d)}{\sqrt{R^2+(z-d)^2}}\right]_{-D}^{0}$$

It is important here to notice that in this case d << D (we recall that d is the distance of the adsorbed molecule from the surface, while D is the sample thickness), so that the field does not depend on d, but only on (D/R), i.e. the sample aspect ratio.

In our case, the sample dimensions were D=1mm, R=5 mm, so that we eventually obtain:

$$B_x(0) = -\frac{\mu_0 \mu_B}{4\pi V_{cell}} \frac{\pi D}{\sqrt{R^2 + D^2}} \sin 70° = -84mT \frac{\pi D}{\sqrt{R^2 + D^2}} \sin 70° = -50mT$$

and

$$B_z(0) = \frac{\mu_0 \mu_B}{4\pi V_{cell}} \frac{2\pi D}{\sqrt{R^2 + D^2}} \cos 70° = 84mT \frac{2\pi D}{\sqrt{R^2 + D^2}} 2\pi \cos 70° = 35mT$$

We here highligth two important aspects of this calculation:

- the non-negligible value of the dipole field here calculated is strictly related to the macroscopic thickness of our sample; this means that for systems were the magnetic substrate is given by a thin Nickel film, the stray field would be reasonably negligible (see [s10]).
- These values are exact for a molecule adsorbed in the center of the sample surface, and as long as the effect of the sample multi-domain structure can be neglected (i.e. when the Nickel magnetization is saturated).

A precise evaluation of the intensity of the stray field would require both a detailed knowledge of closure-domain distribution at the surface (which is indeed quite a demanding issue) and the calculation of the field dependence of the sample axis distance ρ. We nonetheless believe that this simple calculation provides a rough, but sensible estimate of the field order of magnitude, which is the same as that of Beff . Moreover, it is important to observe that, while B_x is anti-parallel to the Ni magnetization (thus mimicking an anti-ferromagnetic coupling along the sample surface), B_z is parallel to it (thus mimicking a ferromagnetic coupling along the normal to the surface).

Supplementary References

[S01] R. Addou, A. Dahal, P. Sutter and M. Batzill, Monolayer graphene growth on Ni(111) by low temperature chemical vapor deposition, *Applied Physics Letters*, 2012, **100,** 021601.

[S02] J. Lahiri, T. S. Miller, A. J. Ross, L. Adamska, I. I. Oleynik and M. Batzill, Graphene growth and stability at nickel surfaces, *New Journal of Physics*, 2011, **13** 025001.

[S03] A. Grüneis, K. Kummer and D. V. Vyalikh, Dynamics of graphene growth on a metal surface: a time-dependent photoemission study, *New Journal of Physics,* 2009, **11** 073050.

[**S04**] A. Varykhalov, J. Sa´nchez-Barriga, A. M. Shikin, C. Biswas, E. Vescovo, A. Rybkin, D. Marchenko, and O. Rader, Electronic and magnetic properties of quasifreestanding graphene on Ni, *Phys. Rev. Lett.*, 2008, **101**, 157601.

[**S05**] D. Marchenko, A. Varykhalov, M.R. Scholz, G. Bihlmayer, E.I. Rashba, A. Rybkin, A.M. Shikin and O. Rader, Giant Rashba splitting in graphene due to hybridization with gold, *Nature Comm.*, 2012, **3**, 1232.

[S06] S.Y. Zhou, G. H. Gweon, and A. Lanzara, Low energy excitations in graphite: The role of dimensionality and lattice defects, *Ann. Phys. (N.Y.),* 2006, **321**, 1730, and refs. therein.

[S07] A. Bostwick, T. Ohta, T. Seyller, K. Horn, E. Rotenberg, Quasiparticle dynamics in graphene, *Nature Phys*., 2007, **3**, 36.

[S08] A. Candini, D. Klar, S. Marocchi, V. Corradini, R. Biagi, V. de Renzi, U. del Pennino, F. Troiani, V. Bellini, S. Klyatskaya, M. Ruben, K. Kummer, N. B. Brookes, H. Huang, A. Soncini, H. Wende, M. Affronte, Spin-communication channels between Ln(III) bis-phthalocyanines molecular nanomagnets and a magnetic substrate, *Scientific Reports*, 2016, **6**, 21740.

[S09] S. Marocchi, A. Candini, D. Klar, W. Van den Heuvel, H. Huang, F. Troiani, V. Corradini, R. Biagi, V. De Renzi, S. Klyatskaya, K. Kummer, N. B. Brookes, M. Ruben, H. Wende, U. del Pennino, A. Soncini, M. Affronte, and V. Bellini, Relay-Like Exchange Mechanism through a Spin Radical between TbPc2 Molecules and Graphene/Ni(111) Substrates, *ACS Nano*, 2016, **10**, 9353-9360.

[s10] A. Lodi Rizzini et al., *Phys. Rev. Lett.*, 2011, **107** (17), 177205.